Published in final edited form as:
Nat Neurosci. 2008 July ; 11(7): 807–815. doi:10.1038/nn.2145.

Rapid and modifiable neurotransmitter receptor dynamics at a neuronal synapse *in vivo*

Corey M McCann[1], **Juan Carlos Tapia**[1], **Han Kim**[1], **Jay S Coggan**[2], and **Jeff W Lichtman**[1]

1*Department of Molecular & Cellular Biology, Harvard University, 7 Divinity Ave., Cambridge, Massachusetts 02138, USA.*

2*Computational Neurobiology Laboratory, The Salk Institute, 10010 N. Torrey Pines Rd., La Jolla, California 92037, USA.*

Abstract

Synaptic plasticity underlies the adaptability of the mammalian brain, but has been difficult to study in living animals. Here we imaged the synapses between pre- and postganglionic neurons in the mouse submandibular ganglion *in vivo*, focusing on the mechanisms that maintain and regulate neurotransmitter receptor density at postsynaptic sites. Normally, synaptic receptor densities were maintained by rapid exchange of receptors with nonsynaptic regions (over minutes) and by continual turnover of cell surface receptors (over hours). However, after ganglion cell axons were crushed, synaptic receptors showed greater lateral mobility and there was a precipitous decline in insertion. These changes led to near-complete loss of synaptic receptors and synaptic depression. Disappearance of postsynaptic spines and presynaptic terminals followed this acute synaptic depression. Therefore, neurotransmitter receptor dynamism associated with rapid changes in synaptic efficacy precedes long-lasting structural changes in synaptic connectivity.

The mechanisms that maintain and modify synaptic structure and function *in vivo* remain poorly understood. In a number of systems it appears that an important regulator of a synapse's efficacy is the density of postsynaptic neurotransmitter receptors[1]. From *in vitro* studies, there seem to be two distinct modes by which neurotransmitter receptor density can be altered: (i) diffusion-limited lateral mobility, which exchanges neurotransmitter receptors between synaptic and nonsynaptic areas[2], and (ii) turnover, which removes receptors from, and inserts receptors into, the plasma membrane[3]. To maintain synaptic strength at a constant level, both these mechanisms are thought to operate at a steady state, maintaining a constant density of postsynaptic neurotransmitter receptors. On cultured neurons, however, this equilibrium can be experimentally disrupted, leading to alterations in neurotransmitter receptor number[4–6].

Although much less is known concerning the regulation of neurotransmitter receptor density on neurons *in vivo*, it is likely to be important. Studies of neuromuscular junctions (NMJs) *in vivo* show that there are dynamic mechanisms that both maintain and rapidly alter neurotransmitter receptor density at synapses[7,8]. Moreover, receptor density on neurons *in vivo* can be rapidly altered by certain perturbations such as axotomy[9], which induces synaptic depression and neurotransmitter receptor loss from the postsynaptic sites of the injured

Correspondence should be addressed to J.W.L. (E-mail: jeff@mcb.harvard.edu).

AUTHOR CONTRIBUTIONS

C.M.M. and J.W.L. designed the experiments and wrote the manuscript. C.M.M. and H.K. conducted the imaging experiments. J.C.T. and J.S.C. conducted the electrophysiology experiments.

neurons[10]. In addition, axotomy results in long-lasting structural changes that affect the number of synapses[11]. As such, this perturbation may be a good *in vivo* model for the ways synaptic plasticity alters the structure and function of connections between nerve cells.

Here we studied neurons in the submandibular ganglion (SMG) because it is optically accessible *in vivo* and because neurotransmitter receptor dynamics can be monitored using a fluorescently tagged ligand[12]. Using this preparation, we observed the dynamic events that maintain and modify synaptic neurotransmitter receptor density at synapses. Our studies provide *in vivo* evidence for a transition from synaptic depression to long-lasting structural changes in synaptic connectivity.

RESULTS

AChRs visualized on submandibular ganglion cells *in vivo*

In the adult submandibular ganglion (SMG), preganglionic neurons branch to form a basket-like arrangement of synapses that surrounds postganglionic neurons (Fig. 1a). Postganglionic neurons lack an elaborate dendritic tree, and therefore the entire complement of synaptic inputs to each neuron can be identified *in vivo* with little ambiguity.

To understand how α7 AChR–containing synaptic sites are organized, we used fluorescent α-bungarotoxin (BTX)[12] and identified three categories of α7 AChR labeling on each ganglion cell. First, some AChR clusters were within 1 μm of preganglionic presynaptic boutons (see, for example, circle in Fig. 1b and **Supplementary Fig. 1a** online). Second, some clusters of AChRs were not associated with synapses (box in Fig. 1b and **Supplementary Fig. 1**). Third, there was fainter, diffuse labeling of the postganglionic cell body and axon hillock that did not extend into the axon (Fig. 1b,c, white and blue arrowheads). The density of AChR labeling was similar at synapse-associated and nonsynatic clusterss (Fig. 1d; nonsynaptic clusters were 93 ± 22% the intensity of synaptic clusters, $n = 28$ cells), whereas the diffuse AChRs were significantly less intense (7 ± 4% the intensity of synaptic clusters, $n = 28$ cells). By measuring the relative areas (Fig. 1e) and integrating intensities (Fig. 1f) of the three receptor populations, we determined that most AChRs on the ganglion cell surface (~70%) were found at synapses. Nonsynaptic AChRs were distributed approximately evenly between nonsynaptic clusters (~18%) and diffuse AChRs (~12%). Antibody staining showed that AChR clusters at presynaptic terminals contained evidence of α3 and β4 neuronal nicotinic AChR subunits. Staining for α3 and β4 AChRs was not present at nonsynaptic clusters (**Supplementary Fig. 1b** and data not shown).

We next examined the functional role of α7 AChRs by adding a saturating dose of BTX to block α7-mediated synaptic currents. As in other autonomic ganglia[13,14], BTX decreased the amplitude of evoked synaptic potentials in the SMG (47 ± 15%, $n = 17$, $P < 0.0044$; Fig. 1g–i). In addition, we noted that in some cells the decay rate of the synaptic potential was also increased. Thus fluorescent BTX can be used to track and label physiologically relevant neurotransmitter receptors at this neuronal synapse *in vivo*.

Maintenance of synaptic AChR clusters

We labeled and imaged postganglionic AChRs *in vivo* for several days to study the stability of synaptic and nonsynaptic clusters. Whereas the location of postsynaptic AChRs remained stable (**Supplementary Fig. 2a** online, white circle), nonsynaptic AChR clusters were significantly more dynamic, with both new appearances and disappearances over several days (**Supplementary Fig. 2a**, colored rectangles, and **Supplementary Fig. 2b**, $n = 12$ cells). Despite rapid changes in the location of nonsynaptic AChR clusters, the relative distribution of cell surface AChRs between synaptic and nonsynaptic regions remained stable, as would

be expected given the long-term maintenance of preganglionic synapses[15] (**Supplementary Fig. 2c**, $n = 12$ cells).

Rapid lateral diffusion of cell surface AChRs

The stability of synaptic AChR clusters raises the possibility that the individual receptor molecules that comprise synaptic clusters may themselves be quite stable. We therefore examined their lateral mobility by quantifying fluorescence recovery after photobleaching (FRAP) of AChRs labeled with fluorescent BTX[16] (see **Supplementary Fig. 3** online for BTX binding affinity controls and Methods for details).

After bleaching small (1-μm^2) regions of AChR fluorescence, we observed rapid recovery of the fluorescent signal (Fig. 2a,b). Several properties of the fluorescence recovery were consistent with membrane diffusion of BTX-labeled AChRs. For example, the recovery showed an exponential profile (Fig. 2c) and was dependent on the size of the bleached area (Fig. 2d). Furthermore, bleaching the entire cell blocked fluorescence recovery ($n = 11$ cells), and when we bleached all fluorescence except for a small region, that region was observed to dim rapidly ($n = 3$ cells), presumably as a result of the net diffusion of labeled receptors into unlabeled regions.

We compared fluorescence recovery for synaptic and nonsynaptic AChR clusters by bleaching similarly sized spots on the same cell (circle and square, respectively, in Fig. 2a). Synaptic AChR clusters recovered tenfold more rapidly than has been reported at the NMJ[17] (Fig. 2b–d, $t_{1/2}$ recovery for a 1-μm^2 spot = 41 ± 7 min, $n = 21$ cells), but significantly more slowly than nonsynaptic AChR clusters did (Fig. 2b–d, $t_{1/2}$ recovery for a 1-μm^2 spot = 11 ± 4 min, $n = 21$ cells).

To assay for receptor mixing between synaptic and nonsynaptic pools, we bleached large regions of synaptic receptors and then quantitatively imaged nonsynaptic receptor clusters over time ($n = 5$ cells) (Fig. 3a–c). After bleaching synaptic receptors, we observed fluorescent recovery of the bleached area (Fig. 3b, white rectangle, and Fig. 3c, purple diamonds). However, unbleached nonsynaptic receptor clusters on the same cell rapidly dimmed (Fig. 3b, white circle, and Fig. 3c, green diamonds). In contrast, the fluorescence intensity of nonsynaptic receptors on neighboring, unbleached cells remained stable throughout the course of the experiment (Fig. 3b, arrows, and Fig. 3c, blue diamonds). The rapid dimming of unbleached nonsynaptic receptors in the presence of large areas of bleached synaptic receptors suggests that synaptic receptors can intermix with receptors in nonsynaptic regions of the cell surface.

Rapid turnover of cell surface AChRs

To measure the turnover rate of surface AChRs in the SMG, we adapted quantitative fluorescence and pulse-chase techniques to measure cell surface receptor turnover *in vivo*[7,18,19] (see Methods). Twelve hours after labeling of cell surface AChRs, most labeling was no longer visible on the membrane and instead appeared as small intracellular puncta (Fig. 4a, red staining). When a second colored fluorescent conjugate of BTX was added, we observed newly inserted AChRs in clusters on the cell surface (Fig. 4a and inset, green staining; see also **Supplementary Fig. 3** for control experiments). Thus not only is there more rapid mobility in the SMG, but the amount of AChR internalization and insertion that would be measured in weeks at the NMJ[7,20] can occur over hours in the SMG.

To measure the lifetime of cell surface AChRs, we labeled receptors with fluorescent BTX and then quantitatively imaged them over time *in vivo*. Receptor labeling became dim and intracellular staining increased in intensity over several hours (Fig. 4b,c and insets). The rate of dimming was independent of BTX concentration and hence of the fraction of labeled cell

surface AChRs (**Supplementary Fig. 3c**). The rate of loss of surface AChRs ($t_{1/2}$ = 350 ± 47 min, n = 60 cells) was considerably more rapid (~60-fold) than the turnover of AChRs at the NMJ.

We also measured the insertion of new AChRs into the cell membrane (Fig. 4b, last panel). After saturation with labeled BTX and several hundred minutes of waiting, cell surface AChRs dimmed by approximately 50% (see above); however, when more labeled BTX was applied, the clusters returned to the initial intensity (Fig. 4b, last panel; Fig. 4c, dark gray squares, n = 16 cells). This result indicates that BTX labeling did not have an effect on cell surface AChR density and is compatible with a model in which, normally, endocytosed receptors are replaced by an equal number of new AChRs to maintain cell surface AChR density at constant levels.

Some neurotransmitter receptors have been shown to be internalized at sites that are far from synapses[21,22]. However, hours after labeling cell surface receptors, we observed AChR puncta within the confines of synaptic clusters (Fig. 4a inset, red staining). To ask how neurotransmitter receptors on the cell surface are removed, we imaged receptor internalization at high temporal resolution (Fig. 4d and Supplementary Movie 1 online). Six to twelve hours after labeling receptor clusters, we observed the sudden appearance of multiple brightly fluorescent < 1 μm in diameter puncta within each cluster (Fig. 4a, inset, and Fig. 4d, colorized puncta). These puncta moved laterally, mostly within the confines of individual clusters, for minutes (Fig. 4d, green puncta). Some of these puncta were, however, observed to rapidly move away from a cluster over the course of seconds (Fig. 4d, red puncta). We suspect that these quickly moving fluorescent spots are translocating from the cell surface to the cell interior because these events coincide with both an accumulation of intracellular spots (see Fig. 4a) and a decrease in cell surface staining (see Fig. 4b). When we tracked fluorescent puncta that were intracellular (see, for example, Fig. 4b inset), we found them to be highly mobile and moving in a pattern reminiscent of endosomes[23] (Supplementary Movie 2 online). These results suggest that AChRs are continuously being endocytosed from cell surface receptor clusters and that this process involves the rapid internalization of receptor-rich vesicles that then translocate into the endosomal pathway.

AChR loss underlies synaptic depression after axotomy

One well-known way to induce weakening at a synapse is to damage the postsynaptic cell's axon[9,24]. We found that in the SMG, postganglionic axotomy rapidly reduced evoked synaptic potentials (Fig. 5a–f). Three weeks after axotomy, however, synaptic amplitudes recovered as the damaged axons reinnervated their gland targets. To assess whether the axotomy-induced depression involved pre- and/or postsynaptic changes, we analyzed spontaneous miniature synaptic potentials after axotomy. In the first 3 d after axotomy, the size of miniature synaptic events was significantly reduced (Fig. 5d, 0.60 ± 0.12 mV after axotomy versus 1.30 ± 0.14 mV in age-matched controls, P = 0.0003, n = 7 cells in each category), but quantal content remained comparable to control values (Fig. 5e, 17.11 ± 3.71 after axotomy versus 19.93 ± 1.77 in age-matched controls, P = 0.52, n = 7 cells in each category). These results could mean that less neurotransmitter is packaged in each quantum, that the acetylcholine has less access to the postsynaptic membrane or that the postsynaptic AChRs have disappeared.

Imaging of axotomized neurons suggested that synaptic depression is due to a marked decrease in postsynaptic AChRs (Fig. 5g–k). Three days after axotomy, ganglion cells had lost almost all clustered receptors (Fig. 5g, right column, and Fig. 5k). α7 AChRs were greatly reduced (Fig. 5k), and axotomized neurons also showed reduced amounts of the other two subunits normally associated with synaptic clusters: α3 and β4 (Fig. 5g,k). These latter two receptor subtypes seemed slightly less affected (Fig. 5k). Further supporting the role of postsynaptic receptors in mediating synaptic potentials after axotomy, α7 AChRs returned to postsynaptic cells 3 weeks after axotomy, as synaptic transmission was restored (Fig. 5h).

Because BTX blocks only α7 AChRs, we could use it to physiologically determine the degree to which the loss of α7-containing versus non-α7-containing AChRs contributes to synaptic depression. We added a saturating dose of BTX to axotomized SMG neurons and then measured synaptic potentials. Whereas BTX significantly reduced the amplitude of synaptic potentials in control cells (~50% reduction) (Fig. 5f, first two bars, and Fig. 1g–i), 3–8 d after axotomy BTX had no attenuating effect on synaptic transmission (Fig. 5f, last two bars). These results suggest that after axotomy there are few α7 containing receptors participating in synaptic transmission.

Notably, despite the reduction in synaptic amplitude, the basket-like preganglionic input to axotomized cells appeared unchanged in terms of their structure and number of synaptic boutons (Fig. 5i,j). In addition, as indicated by immunohistochemistry, the nerve terminals contained normal amounts of two synaptic vesicle proteins (SV2 and synaptotagmin-2; Fig. 5j,k).

AChR loss via increased mobility and decreased insertion

Following axotomy, we monitored the distribution of AChRs on the postganglionic cell surface to determine how AChR clusters disappeared (Fig. 6). Twelve to twenty-four hours after axotomy, synaptic clusters seemed largely unchanged in terms of shape and area, but their fluorescence intensity was diminished by ~35% (n = 22 cells) as compared to that of synaptic AChR clusters on control ganglion cells (Fig. 6a). This loss of AChRs at synaptic clusters contrasted with an increase in fluorescence intensity both at nonsynaptic clusters and in the diffuse receptor pool (~50% increase, n = 22 cells) (Fig. 6b, compare intensity of circled and boxed regions). By 48 h after axotomy, the total number of surface AChRs had declined by ~50% (n = 20 cells) (Fig. 6d). In addition, individual clusters decreased in area, and there were few if any nonsynaptic clusters or signs of any remaining diffuse receptor fluorescence (Fig. 6d). By 72 h after axotomy, most ganglion cells did not show any BTX labeling (n = 40 cells) (Fig. 5g,h).

To learn how this profound change in cell surface receptor density came about, we examined the lateral mobility and turnover of AChRs after axotomy. Twelve to twenty-four hours after axotomy—when, as mentioned above, AChRs were redistributed from synaptic to non-synaptic sites—synaptic AChRs became significantly more mobile in the cell membrane (FRAP for a 1-μm^2 spot, $t_{1/2}$ = 40 ± 6 min for control and 21 ± 8 min for axotomy; Fig. 6c, n = 10 cells). However, at this time the mobility of nonsynaptic AChRs was unchanged (FRAP for a 1-μm^2 spot, $t_{1/2}$ = 10 ± 3 min versus 12 ± 5 min; Fig. 6c, n = 10 cells) and the rate of internalization of surface AChRs (by fluorescence decay measurement) and the rate of AChR insertion into the plasma membrane (by relabeling assay) were also unchanged from those of controls (data not shown). At 48 h after axotomy, the lateral dynamism of AChRs was similar to that observed at 24 h (data not shown), but the turnover of cell surface AChRs was perturbed (Fig. 6e,f and **Supplementary Fig. 4** online). In normal ganglion cells, internalized receptors are replaced by an equal number of new AChRs, maintaining the steady-state surface receptor density (Fig. 4b,c and Fig. 6f). At 48 h after axotomy, however, the rate of AChR insertion had decreased significantly (18 ± 15% in axotomy versus 98 ± 10% replacement in controls, n = 16 cells), but the internalization rate was not significantly different from control values ($t_{1/2}$ = 335 ± 70 min in axotomy, n = 8 cells versus 350 ± 47 min in controls). This mismatch between insertion and internalization explains the large-scale loss of surface AChRs.

Loss of PSD-93 precedes AChR density changes

Because components of the postsynaptic density are thought to regulate neurotransmitter receptor stability[25,26], we asked whether the localization of PSD-93, the chief postsynaptic density protein in SMG neurons[27] and a putative binding partner of AChR α7 (ref. 28), is

related to the stability of α7 AChRs (Fig. 7). In adult postganglionic neurons, PSD-93 labeling was present in small spines on the postganglionic cell soma and axon hillock (Fig. 7a–c; see white arrow and inset in Fig. 7c). These sites were precisely apposed to presynaptic terminals (Fig. 7b) and excluded from nonsynaptic regions (**Supplementary Fig. 1c,d**, and see ref. [27]). When we co-labeled AChR α7 and PSD-93, we observed two populations of AChR clusters: clusters that contained PSD-93 labeling within them and clusters that did not (Fig. 7e, circle and square, respectively). This result was expected because PSD-93 is only present at synaptic sites and most ganglion cells have both synaptic and nonsynaptic AChR clusters.

Given the loss of AChRs after axotomy, we were interested to learn whether PSD-93 also was altered. Two to three days after axotomy, we observed almost complete loss of PSD-93 from postganglionic spines (Fig. 7d, white arrow and inset). We also observed an increase in the presence of PSD-93 spots that now diffusely filled the cytoplasm of the postganglionic neuron (Fig. 7d, yellow arrow, and Fig. 7f). This change in PSD-93 location was already evident by 24 h after axotomy, and by 2 d there was nearly complete loss of synaptic PSD-93 puncta (Fig. 7g,i). Notably, the loss of PSD-93 preceded the loss of AChRs (Fig. 7f–i). At 24 h after axotomy, PSD-93 showed 60 ± 11% reduction at synaptic sites (n = 17 cells), but BTX staining showed near-normal levels of AChRs on the cell surface (10 ± 15% reduction, n = 25 cells) (Fig. 7g–i). AChR loss still lagged behind PSD-93 loss at 48 h after axotomy, but both reached near-maximal levels by 72 h (Fig. 7f–i).

Synapse elimination after postsynaptic AChR loss

The evidence above showing reduction in quantal size without change in quantal content at day 1–3 after axotomy (Fig. 5d,e) suggests that the initial synaptic depression after axotomy is due to a large-scale disappearance of cholinergic neurotransmitter receptors. However, this alteration does not fully explain the physiological changes recorded after 1 week. At 1 week after axotomy all cells recorded showed a decrease in quantal content (Fig. 5e). Moreover, at this time many postganglionic neurons were now completely unresponsive to preganglionic stimulation (Fig. 8a). Images of neurons 1 week after axotomy suggested a reason for these alterations: whereas presynaptic terminals are normally concentrated on spines (Fig. 8b and inset; see also Fig. 7a,b), 1 week after axotomy ganglion cells often lacked postsynaptic spines (Fig. 8c, blue labeling). In addition, presynaptic terminals were no longer present (Fig. 8c, green labeling).

We characterized the synapse loss further in order to better understand this kind of synapse elimination. We imaged neurons in a yellow fluorescent protein (YFP)-expressing mouse line that still possessed YFP-labeled preganglionic input 7–10 d after axotomy. In these cases, we found preganglionic axons that terminated in many bulb-tipped endings, and in some cases there was evidence of disconnected presynaptic debris (Fig. 8d, boxed regions). Both bulbs and debris are characteristic of presynaptic retraction in naturally occurring synapse elimination during development[29]. Time-lapse and fixed time-point imaging showed that during the first 5 d after axotomy, presynaptic inputs to postganglionic neurons were unchanged and stably maintained (Fig. 8e, first three panels; Fig. 8f, first two bars), but after 7 d, presynaptic loss was evident (Fig. 8e, last panel, red box; Fig. 8f, last bar).

DISCUSSION

In these studies we took advantage of recently developed techniques to fluorescently label and image pre- and postsynaptic sites on autonomic neurons in living mice[12]. With this approach, we observed the ways in which neurotransmitter receptors at synapses are regulated *in vivo*. The behavior of neurotransmitter receptors at autonomic synapses contrasts significantly with the more stable behavior of AChRs at NMJs on skeletal muscle fibers. We found, for example, that whereas neuromuscular AChRs at synapses have a half-life of approximately 14 d (ref.

7), AChRs on SMG neurons turn over ~60 times more rapidly ($t_{1/2}$ = 0.24 d). Moreover, the lateral diffusion of AChRs on SMG neurons is also ~10 times faster than that of AChRs at the NMJ[17]. In addition, we saw that most ganglion cells possessed a number of receptor clusters that were not innervated. Although such clusters are uncommon on muscle fibers[30], in neurons several subtypes of neuronal neurotransmitter receptors have been shown to cluster at uninnervated sites[31,32]. Our evidence suggests that exchange of AChRs occurs between the synaptic and nonsynaptic regions. This mobility of receptors may provide a means of rapidly changing receptor density at synapses, which could modify synaptic efficacy.

We explored the potential role of AChR dynamism in the synaptic depression that begins shortly after axotomy of postsynaptic cells. Over the first several days after axotomy, we observed an approximately tenfold decrease in postsynaptic neurotransmitter receptor density. The results were based on changes in the α7 subunit; we do not know whether other subunits (for example, β2) also undergo loss. This loss of AChRs was associated with a sequence of alterations in the ganglion cell. First, we observed that PSD-93, a postsynaptic density protein, disappeared from synaptic sites. Then synaptic AChRs increased in lateral mobility and were lost from synaptic sites. We next noted a marked reduction in the rate of new AChR insertion to the cell surface (the rate of AChR removal remained unchanged throughout the process). The disequilibrium between receptor insertion and receptor removal led to a net reduction in the total number of cell surface AChRs in axotomized neurons. Our physiological assays of axotomized cells suggest that synaptic depression involves the loss of α7-containing AChRs and starts at the same time that AChRs begin migrating away from synapses. This correlation is compatible with the idea that changes in AChR density are related to the decreased efficacy of synaptic transmission. Moreover, during the first several days, receptor loss is not matched by changes in the preganglionic nerve terminal; at this stage presynaptic terminals contain normal amounts of synaptic vesicle proteins and remain attached to postsynaptic cells. These results argue that changes in neurotransmitter receptor dynamics (turnover and mobility) may be instrumental in rapidly depressing synaptic transmission *in vivo*.

Over a longer time scale, our results indicate that synaptic depression is followed by long-lasting changes in synaptic connectivity. We noted that several days after axotomy, many postganglionic neurons became completely unresponsive to preganglionic stimulation. At this time, postsynaptic spines were no longer evident and preganglionic axon terminals began to thin and retract. Ultimately synapse loss was widespread. This frank synapse elimination contrasts with the marked stability of synaptic connections that we have observed in the normal adult SMG[15]. Therefore, the synapse loss after axotomy is explained by a deficit in synaptic maintenance rather than a deficiency in ongoing synapse formation. These data thus provide evidence for a transition from depression to elimination of neuro-neuronal synapses *in vivo*.

How might postganglionic axotomy result in the elimination of depressed synaptic connections? One recent study argues that retrograde signaling is necessary for the maintenance of neuromuscular synapses *in vivo*[33]. The nature of this retrograde maintenance pathway is unknown, but candidates include synaptic adhesion molecules and trophic factors. The role of trophic factors after axotomy is supported by evidence that administration of nerve growth factor can prevent synaptic depression in axotomized superior cervical ganglion neurons[34].

In summary, axotomy leads to rapid functional depression followed by long-lasting synapse elimination. The progression demonstrated here may provide a framework for understanding other, similar-appearing forms of synapse loss that occur during normal development[35] and aging[36].

METHODS

BTX labeling

Cell surface AChRs were labeled as reported previously[12]. Briefly, animals were anesthetized, intubated and mechanically ventilated. A ventral midline incision was made in the neck and the salivary ducts exposed by blunt dissection. A 5 μg ml^{-1} mixture of fluorescent BTX (Invitrogen) in lactated Ringer's solution (Baxter) was added to the neck and maintained for 30 min–3 h (0.5 μg ml^{-1} BTX for 30 min was used in experiments involving nonsaturating labeling). Unbound BTX was removed by a brief wash with a continuous perfusion of Ringer's solution. SMGs were then either fixed with paraformaldehyde (PFA) and mounted on slides or imaged live.

Antibody staining

Tissue was prepared for staining by first intracardially perfusing mice with 4% PFA. Tissue was then postfixed in 2% or 4% PFA for 10–30 min and dissected to reveal the SMG. SMGs were first incubated in 3% BSA and 1% Triton X-100 to block nonspecific antibody binding. Antibody labeling was conducted in the same solution. The following primary antibodies and dilutions were used: rabbit anti-chapsyn 110 (PSD-93) (1:1,000, Chemicon), chicken anti–green fluorescent protein (anti-GFP; 1:1,000, Aves Lab), goat anti-AChR α7 (1:200, Santa Cruz Biotechnology), znp-1 (1:200, Zebrafish International Resource Center, Eugene, Oregon, USA), SV2 (1:10, Developmental Studies Hybridoma Bank, Iowa City, Iowa, USA), and rabbit anti-AChR α3 (1:100) and rabbit anti-AChR β4 (1:250) (both gifts of G. Feng, Duke University). Primary antibodies were added for 12–18 h and then washed eight times for 60 min each time in lactated Ringer's solution (Baxter). For secondary antibodies, we used donkey anti-rabbit–Alexa Fluor 555 (1:500, Invitrogen), goat anti-rabbit–Cy3 (1:500; Jackson ImmunoResearch, West Grove, PA, USA), and goat anti-chicken IgG–Alexa Fluor 488 (1:500), goat anti-mouse IgG1–Alexa Fluor 568 (1:1,000), goat anti-mouse IgG2a–Alexa Fluor 647 (1:500), donkey anti-goat–Alexa Fluor 647 (1:500) and donkey anti-goat Alexa Fluor 488 (1:500) (all from Invitrogen). Secondary antibody staining was performed for 12–18 h and then washed four times for 60 min in lactated Ringer's solution (Baxter). After antibody staining and washing, we mounted SMGs on slides and imaged them using an FV1000 confocal microscope (Olympus).

In vivo imaging

In vivo imaging was conducted as reported previously[37]. Briefly, after anesthesia and intubation, a ventral midline incision was made in the neck and SMGs were exposed. AChRs were labeled with Alexa-647–BTX (Invitrogen) (as above), and then small metal retractors were used to lift and stabilize the salivary ducts. Postganglionic neurons were identified using oblique illumination, and fluorescent structures were imaged using an upright microscope connected to either a CCD camera (Retiga SRV, QImaging) or a laser scanning confocal microscope (Zeiss LSM 510 Meta). All procedures were approved by the Institutional Animal Care and Use Committee of Harvard University (Cambridge, Massachusetts, USA). All *in vivo* images were taken with a Zeiss 63× water-immersion (1.0 NA) objective. Twelve-bit confocal image stacks were acquired at or beyond the Nyquist limit (0.3–0.5 μm steps, 1,024 × 1,024 pixels). All images were taken using very low laser power to minimize photobleaching. For photobleaching experiments, a small region of interest (ROI) was selected using the Zeiss LSM 510 software and that region was exposed to laser light until it was no longer fluorescent. Single-session and multiday time-lapse imaging sessions were carried out as previously described[37]. An index of stability was calculated by determining the probability that a given cluster type would be present on multiple imaging sessions (1 = maintained, 0 = eliminated).

Quantitative imaging

Quantitative time-lapse imaging procedures were modified from previous studies[37]. We imaged a fluorescent standard before and after each imaging session to detect fluctuations in laser intensity, photomultiplier tube sensitivity and irregularities in the field of view. Background values, calculated by defocusing from a labeled region, were subtracted from images. In all cases, at the near-infrared wavelengths imaged (~633 nm), all of these values (drift and background) were minimal and could be discounted.

All data analysis was performed using Metamorph software (Universal Imaging). Intensities of fluorescent puncta, imaged beyond the Nyquist limit, were measured by centering ROIs on single optical sections and obtaining the mean pixel value in each particular region. Axial planes above and below the ROI were similarly analyzed and the data from the three planes averaged. Data was recorded and analyzed in Microsoft Excel.

Nerve crush

After anesthesia, the salivary ducts were exposed and postganglionic axons were crushed by manually compressing the salivary ducts where they exit the salivary gland. Animals were sutured closed and allowed to recover before subsequent experiments were done.

Electrophysiology

Adult mice (~6 weeks) were anesthetized (ketamine/xylazine, 1.7 mg per kg body weight) and perfused with cold (4 °C) extracellular solution. The lingual nerve, containing the preganglionic axons and salivary ducts that support the ganglion neurons, was dissected out and placed in a recording chamber as previously described[35]. The preparation was continuously superfused (~2 ml min^{-1}) with an oxygenated extracellular solution containing (in mM): 150 NaCl, 5 KCl, 10 $CaCl_2$, 1 $MgCl_2$, 10 HEPES, 10 glucose (pH 7.4). Micropipettes (borosilicate glass) with resistances of 65 MΩ (Sutter Instruments Puller P-97) and filled with 1 M KCl were used for intracellular impalements. Recordings were acquired with Axoscope 9 using Axopatch 1D amplifier, digitized (Digidata 1322A) and stored for offline analysis (all equipment from Axon Instruments). Evoked synaptic potentials (ESPs) were induced after stimulation (Grass Stimulator S88, Grass Technologies) of the lingual nerve (suction electrode). Analysis of ESPs and spontaneous miniature synaptic potentials were carried out using Mini analysis 5.0 Software (Synaptosoft). Only neurons with resting membrane potentials below −50 mV and with no significant drift (±10 mV) were considered for analysis. All values are reported as mean ± s.d. $P < 0.05$ was considered statistically significant (ANOVA test, Origin 6.0).

Supplementary Material

Refer to Web version on PubMed Central for supplementary material.

ACKNOWLEDGMENTS

We thank the members of the J. Lichtman and J. Sanes laboratories for thoughtful comments and discussions. We also thank G. Feng (Duke University) and M. Skok for providing antibodies to AChR subunits. C.M.M. was partially supported by the Medical Scientist Training Program grant at Washington University.

References

1. Malinow R, Malenka RC. AMPA receptor trafficking and synaptic plasticity. Annu. Rev. Neurosci 2002;25:103–126. [PubMed: 12052905]
2. Triller A, Choquet D. Surface trafficking of receptors between synaptic and extra-synaptic membranes: and yet they do move! Trends Neurosci 2005;28:133–139. [PubMed: 15749166]

3. Song I, Huganir RL. Regulation of AMPA receptors during synaptic plasticity. Trends Neurosci 2002;25:578–588. [PubMed: 12392933]
4. Borgdorff AJ, Choquet D. Regulation of AMPA receptor lateral movements. Nature 2002;417:649–653. [PubMed: 12050666]
5. Lu W, et al. Activation of synaptic NMDA receptors induces membrane insertion of new AMPA receptors and LTP in cultured hippocampal neurons. Neuron 2001;29:243–254. [PubMed: 11182095]
6. Beattie EC, et al. Regulation of AMPA receptor endocytosis by a signaling mechanism shared with LTD. Nat. Neurosci 2000;3:1291–1300. [PubMed: 11100150]
7. Akaaboune M, Culican SM, Turney SG, Lichtman JW. Rapid and reversible effects of activity on acetylcholine receptor density at the neuromuscular junction *in vivo*. Science 1999;286:503–507. [PubMed: 10521340]
8. Bruneau EG, Akaaboune M. Running to stand still: ionotropic receptor dynamics at central and peripheral synapses. Mol. Neurobiol 2006;34:137–151. [PubMed: 17220535]
9. Purves D. Functional and structural changes in mammalian sympathetic neurones following interruption of their axons. J. Physiol. (Lond.) 1975;252:429–463. [PubMed: 1206535]
10. Jacob MH, Berg DK. The distribution of acetylcholine receptors in chick ciliary ganglion neurons following disruption of ganglionic connections. J. Neurosci 1988;8:3838–3849. [PubMed: 3193180]
11. Matthews MR, Nelson VH. Detachment of structurally intact nerve endings from chromatolytic neurones of rat superior cervical ganglion during the depression of synaptic transmission induced by post-ganglionic axotomy. J. Physiol. (Lond.) 1975;245:91–135. [PubMed: 165288]
12. McCann CM, Lichtman JW. In vivo imaging of presynaptic terminals and postsynaptic sites in the mouse submandibular ganglion. Dev. Neurobiol 2008;68:760–770. [PubMed: 18383540]
13. Ullian EM, McIntosh JM, Sargent PB. Rapid synaptic transmission in the avian ciliary ganglion is mediated by two distinct classes of nicotinic receptors. J. Neurosci 1997;17:7210–7219. [PubMed: 9295367]
14. Chang KT, Berg DK. Nicotinic acetylcholine receptors containing α7 subunits are required for reliable synaptic transmission in situ. J. Neurosci 1999;19:3701–3710. [PubMed: 10234002]
15. Gan WB, Kwon E, Feng G, Sanes JR, Lichtman JW. Synaptic dynamism measured over minutes to months: age-dependent decline in an autonomic ganglion. Nat. Neurosci 2003;6:956–960. [PubMed: 12925856]
16. Axelrod D, et al. Lateral motion of fluorescently labeled acetylcholine receptors in membranes of developing muscle fibers. Proc. Natl. Acad. Sci. USA 1976;73:4594–4598. [PubMed: 1070010]
17. Akaaboune M, Grady RM, Turney S, Sanes JR, Lichtman JW. Neurotransmitter receptor dynamics studied in vivo by reversible photo-unbinding of fluorescent ligands. Neuron 2002;34:865–876. [PubMed: 12086635]
18. Merlie JP, Changeux JP, Gros F. Acetylcholine receptor degradation measured by pulse chase labelling. Nature 1976;264:74–76. [PubMed: 1004540]
19. Bruneau EG, Macpherson PC, Goldman D, Hume RI, Akaaboune M. The effect of agrin and laminin on acetylcholine receptor dynamics in vitro. Dev. Biol 2005;288:248–258. [PubMed: 16256100]
20. Bruneau E, Sutter D, Hume RI, Akaaboune M. Identification of nicotinic acetylcholine receptor recycling and its role in maintaining receptor density at the neuromuscular junction in vivo. J. Neurosci 2005;25:9949–9959. [PubMed: 16251443]
21. Bogdanov Y, et al. Synaptic $GABA_A$ receptors are directly recruited from their extra-synaptic counterparts. EMBO J 2006;25:4381–4389. [PubMed: 16946701]
22. Ashby MC, et al. Removal of AMPA receptors (AMPARs) from synapses is preceded by transient endocytosis of extrasynaptic AMPARs. J. Neurosci 2004;24:5172–5176. [PubMed: 15175386]
23. Prekeris R, Foletti DL, Scheller RH. Dynamics of tubulovesicular recycling endosomes in hippocampal neurons. J. Neurosci 1999;19:10324–10337. [PubMed: 10575030]
24. Titmus MJ, Faber DS. Axotomy-induced alterations in the electrophysiological characteristics of neurons. Prog. Neurobiol 1990;35:1–51. [PubMed: 2217820]
25. Bats C, Groc L, Choquet D. The interaction between Stargazin and PSD-95 regulates AMPA receptor surface trafficking. Neuron 2007;53:719–734. [PubMed: 17329211]

26. Kim E, Sheng M. PDZ domain proteins of synapses. Nat. Rev. Neurosci 2004;5:771–781. [PubMed: 15378037]
27. Parker MJ, Zhao S, Bredt DS, Sanes JR, Feng G. PSD93 regulates synaptic stability at neuronal cholinergic synapses. J. Neurosci 2004;24:378–388. [PubMed: 14724236]
28. Conroy WG, Liu Z, Nai Q, Coggan JS, Berg DK. PDZ-containing proteins provide a functional postsynaptic scaffold for nicotinic receptors in neurons. Neuron 2003;38:759–771. [PubMed: 12797960]
29. Bishop DL, Misgeld T, Walsh MK, Gan WB, Lichtman JW. Axon branch removal at developing synapses by axosome shedding. Neuron 2004;44:651–661. [PubMed: 15541313]
30. Ko PK, Anderson MJ, Cohen MW. Denervated skeletal muscle fibers develop discrete patches of high acetylcholine receptor density. Science 1977;196:540–542. [PubMed: 850796]
31. Li JH, et al. Developmental changes in localization of NMDA receptor subunits in primary cultures of cortical neurons. Eur. J. Neurosci 1998;10:1704–1715. [PubMed: 9751142]
32. Hutcheon B, Fritschy JM, Poulter MO. Organization of GABA receptor alpha-subunit clustering in the developing rat neocortex and hippocampus. Eur. J. Neurosci 2004;19:2475–2487. [PubMed: 15128401]
33. McCann CM, Nguyen QT, Santo Neto H, Lichtman JW. Rapid synapse elimination after postsynaptic protein synthesis inhibition in vivo. J. Neurosci 2007;27:6064–6067. [PubMed: 17537978]
34. Nja A, Purves D. The effects of nerve growth factor and its antiserum on synapses in the superior cervical ganglion of the guinea-pig. J. Physiol. (Lond.) 1978;277:53–75. [PubMed: 206691]
35. Lichtman JW. The reorganization of synaptic connexions in the rat submandibular ganglion during post-natal development. J. Physiol. (Lond.) 1977;273:155–177. [PubMed: 599418]
36. Coggan JS, et al. Age-associated synapse elimination in mouse parasympathetic ganglia. J. Neurobiol 2004;60:214–226. [PubMed: 15266652]
37. Turney SG, Culican SM, Lichtman JW. A quantitative fluorescence-imaging technique for studying acetylcholine receptor turnover at neuromuscular junctions in living animals. J. Neurosci. Methods 1996;64:199–208. [PubMed: 8699881]

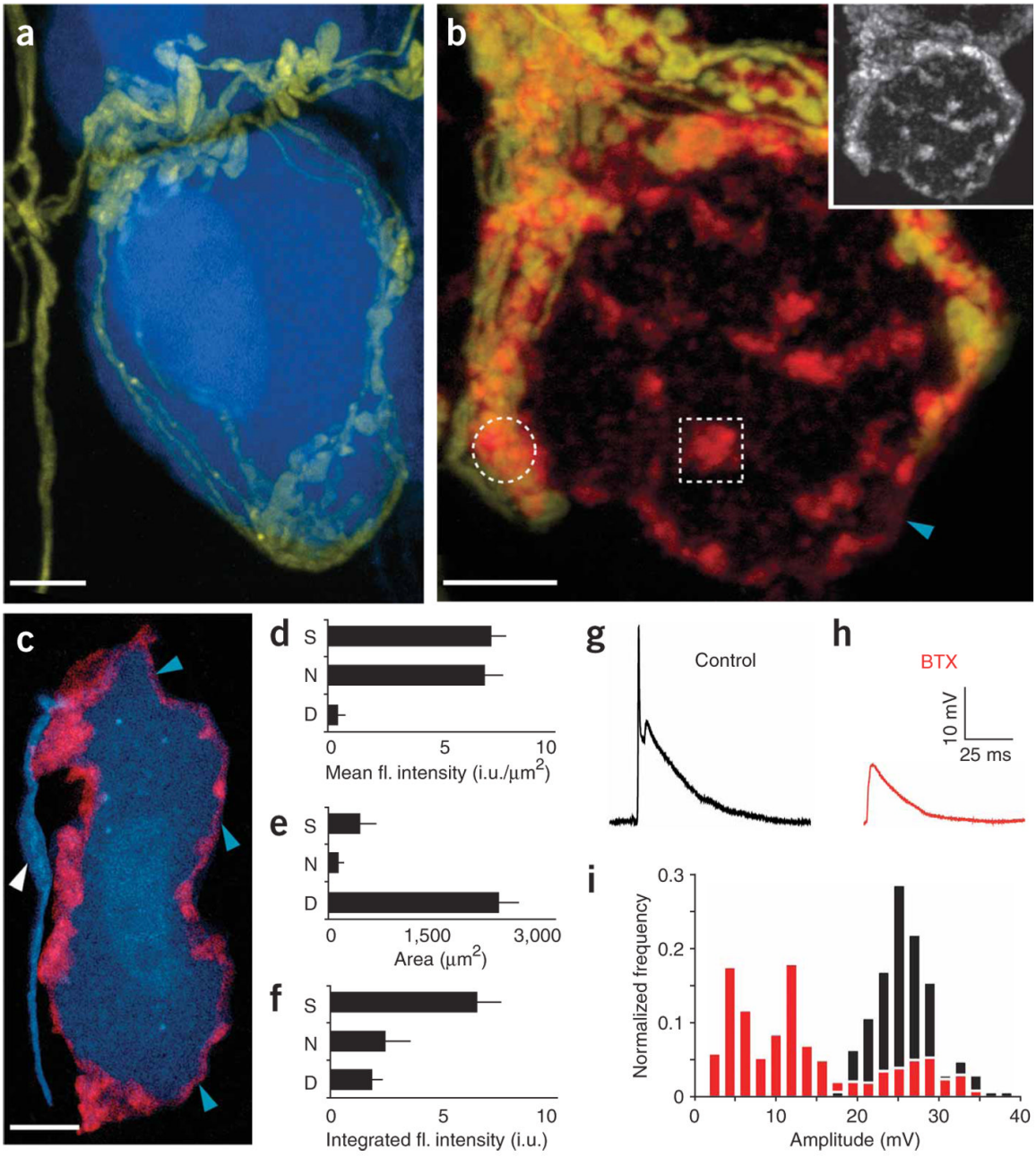

Figure 1. Fluorescently conjugated BTX binds to AChRs on postganglionic neurons in the mouse SMG

(**a**) Basket-like innervation of a single postganglionic neuron from a double transgenic mouse expressing YFP in preganglionic neurons (yellow) and CFP in postganglionic neurons (blue). (**b**) BTX (red) labels the surface of postganglionic neurons in a patchy pattern (inset). Only some BTX-labeled clusters are associated with preganglionic axon terminals (yellow; for example, compare circle and square). Unclustered receptors are also diffusely present (for example, blue arrowhead). (**c**) BTX (blue arrowheads) does not label the axon beyond the initial segment (white arrowhead). Scale bars, 5 μm. (**d–f**) Proportion of BTX-labeled AChRs in synaptic (S), nonsynaptic (N) and diffuse (D) AChR pools. Error bars, s.e.m. fl., fluorescence.

i.u., intensity units. **d** shows the mean intensity of BTX-positive sites in the three receptor populations, **e** the area of each receptor population and **f** the total fluorescence associated with each of the three AChR pools. (**g**) Evoked suprathreshold synaptic potential from stimulation of preganglionic input to a postganglionic neuron. (**h**) The amplitude of evoked synaptic potentials was typically reduced below threshold by BTX application. (**i**) Histogram of evoked synaptic potential amplitudes pooled from multiple, randomly selected cells in control adult SMGs (black bars) and after addition of a saturating dose of BTX (red bars).

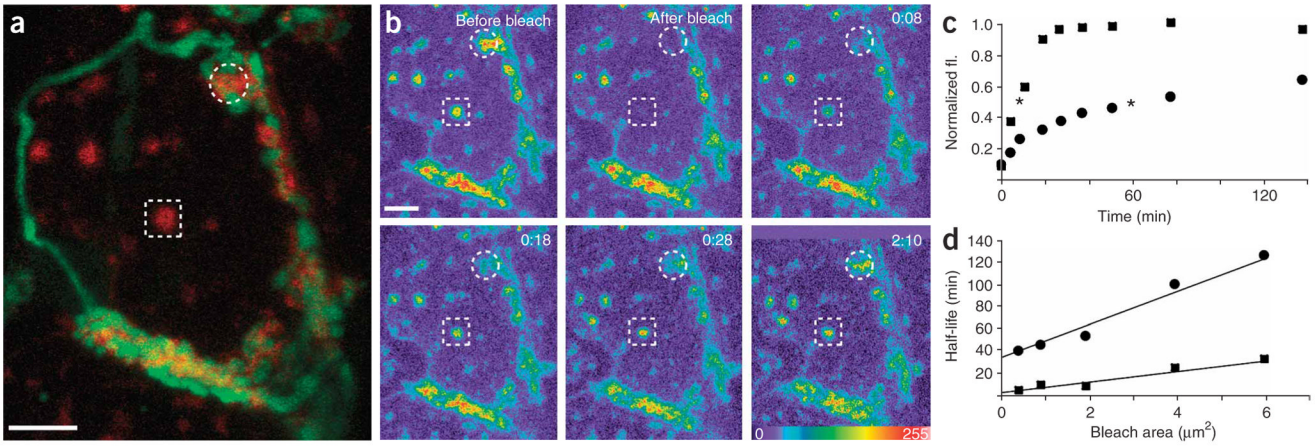

Figure 2. Lateral mobility of AChRs in synaptic and nonsynaptic clusters

(**a**) Similarly sized regions of synaptic (circle) and nonsynaptic (square) AChRs were photobleached (preganglionic axon, green; AChRs, red). (**b**) Time-lapse images of AChR labeling (intensity pseudocolored) before and after bleaching (hr:min). (**c**) Nonsynaptic receptor fluorescence recovered faster than synaptic AChRs. Asterisks indicate half-time of recovery. fl., fluorescence. (**d**) The half-life of recovery was slower for synaptic regions (circles) than for nonsynaptic regions (squares). Scale bars, 5 μm.

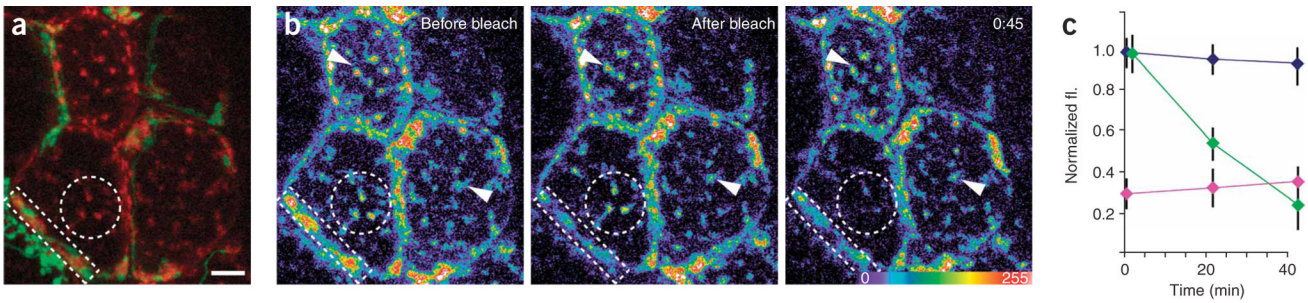

Figure 3. Mixing of synaptic and nonsynaptic AChRs

(**a**) Shown are AChRs sites that are synaptic (associated with green axons) and nonsynaptic (red only). (**b**) After bleaching of synaptic AChRs (rectangle), nonsynaptic AChRs on the same cell (circle) lost fluorescence more rapidly than nonsynaptic AChRs on neighboring cells (arrows) suggesting that bleached synaptic receptors moved into nonsynaptic regions of the same cell. (**c**) Quantification of the experiment shown in **b**. Green diamonds represent nonsynaptic AChR fluorescence (fl.) on the bleached cell, and blue diamonds represent nonsynaptic AChR intensity on neighboring cells. Purple diamonds represent synaptic AChR fluorescence in the bleached region. Error bars, s.e.m. Scale bar, 5 μm.

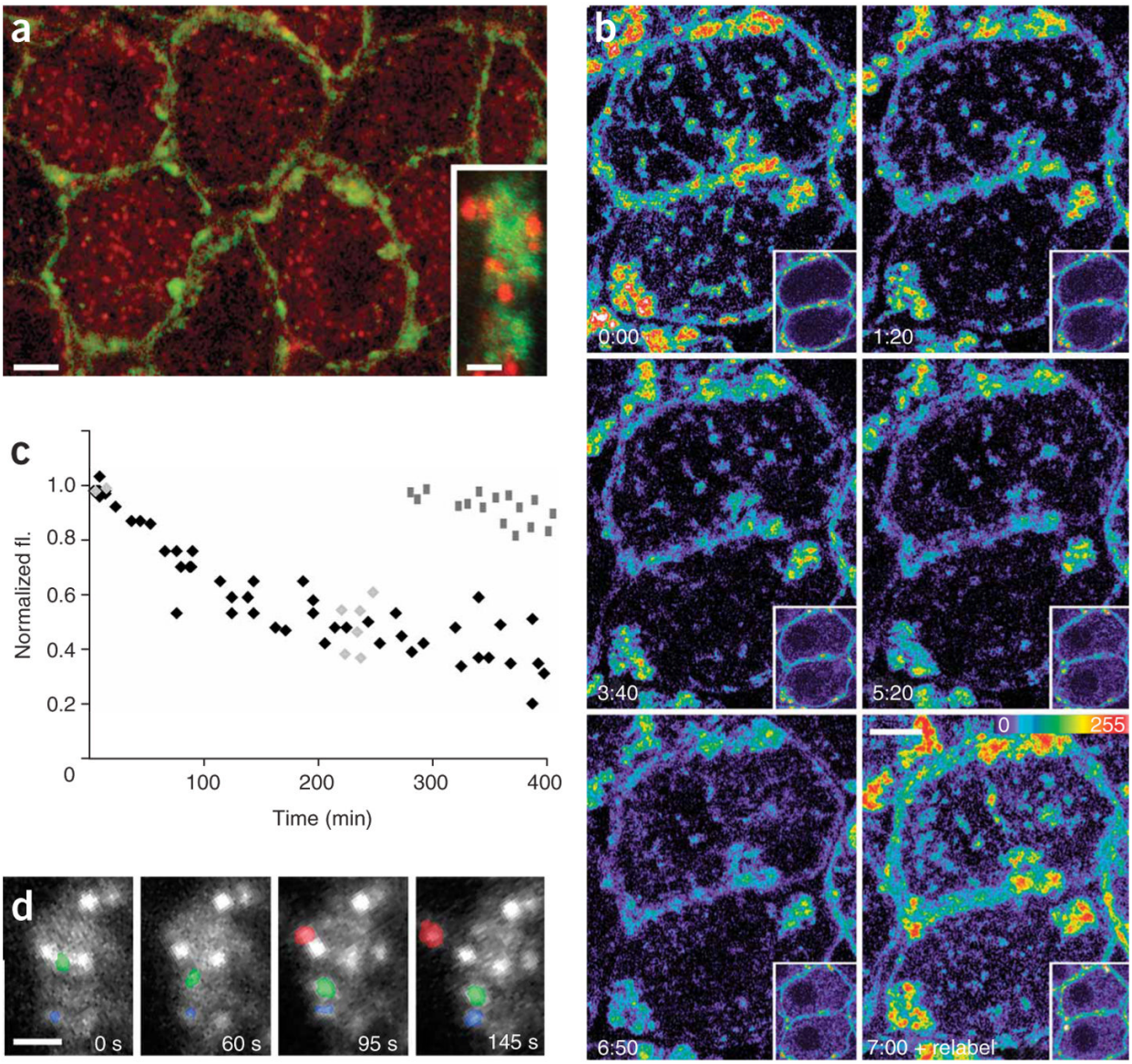

Figure 4. Turnover of cell surface AChRs

(**a**) Evidence for substantial internalization (red) and replenishment (green) of cell surface receptors over 12 h by fluorescent pulse-chase labeling of cell surface AChRs (see text for details). Inset, imaging single synaptic AChR clusters showed that, in and near the sites of new AChRs (green), old AChRs (red) were visible as small round puncta. (**b**) Time-lapse imaging of BTX-labeled AChRs shows progressive dimming of cell surface receptors (first five panels, time 0:00 through 6:50) while intracellular fluorescence steadily increased (see corresponding insets). Cells were relabeled with BTX to highlight newly inserted AChRs. Cell surface labeling returned to the original intensity (last panel, time 7:00 + relabel), indicating that rates of insertion and removal of AChR were similar. (**c**) Quantification of the decay of cell surface BTX labeling from 60 ganglion cells in 14 animals. Each data point represents the pooled fluorescence for a single cell compared to its intensity at time 0. Black diamonds represent data collected continuously (as in **b**) and light gray diamonds represent experiments where the animal was allowed to recover in between images. Dark gray rectangles represent AChRs

immediately after relabeling. (**d**) Time-lapse of an AChR cluster 12 h after BTX labeling, showing rapidly moving (green), stable (blue) and budding (red) puncta (see also Supplementary Movie 1). Scale bars, 5 μm in **a–c**, 2 μm in inset of **a** and in **d**.

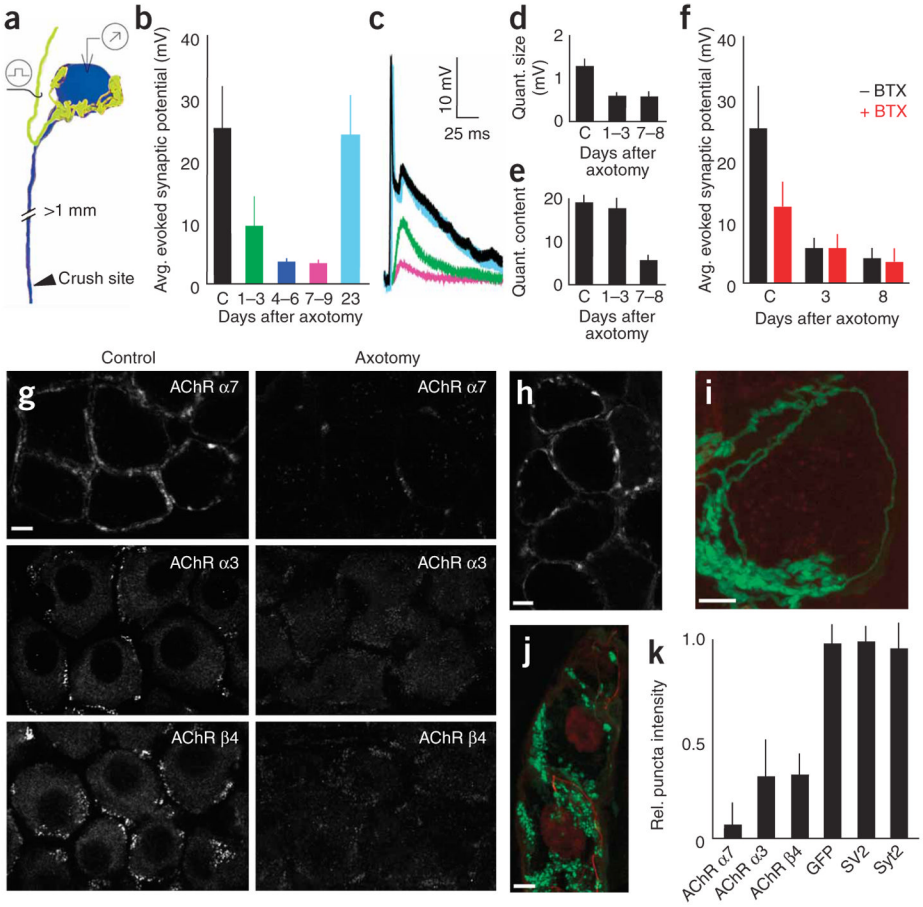

Figure 5. Postsynaptic AChR loss underlies axotomy-induced synaptic depression

(**a**) Schematic depicting the assay for the effects of postganglionic nerve crush on pre- to postganglionic connections (yellow, preganglionic axon; blue: postganglionic neuron). (**b–f**) Physiological analysis of axotomized SMG neurons (**c** shows control values from normal cells). The amplitudes of evoked synaptic potentials were rapidly reduced after axotomy in the SMG (**b**). Also shown are sample traces from control and axotomized neurons (**c**); colors correspond to those of the datasets shown in **b**. Quantal size was reduced soon after axotomy (**d**), whereas quantal content was reduced later (**e**). (**f**) BTX blocked synaptic transmission in control cells (by ~50%) but had no effect on cells that had been axotomized 3–8 d before. (**g**) 72 h after nerve crushing, AChR α7 (BTX) and α3 and β4 AChR subunits (antibodies) were significantly reduced. (**h**) Three weeks after axotomy, synaptic transmission recovered and AChR α7 labeling was again visible. (**i**) 72 h after nerve crush, GFP-labeled preganglionic axons (green) formed normal-appearing basket-like inputs to axotomized ganglion cells even after BTX-labeled AChRs (red) were no longer present. (**j**) The presynaptic marker synaptotagmin-2 (green) and the axonal marker neurofilament (red) remained in preganglionic axon terminals 72 h after postganglionic axotomy. Scale bars, 5 μm in all images. (**k**) At 72 h, presynaptic markers were unaffected by axotomy, but postsynaptic AChRs were significantly reduced. The intensity of synaptic puncta staining in axotomy was compared to controls to give a relative measure. Error bars, s.e.m.

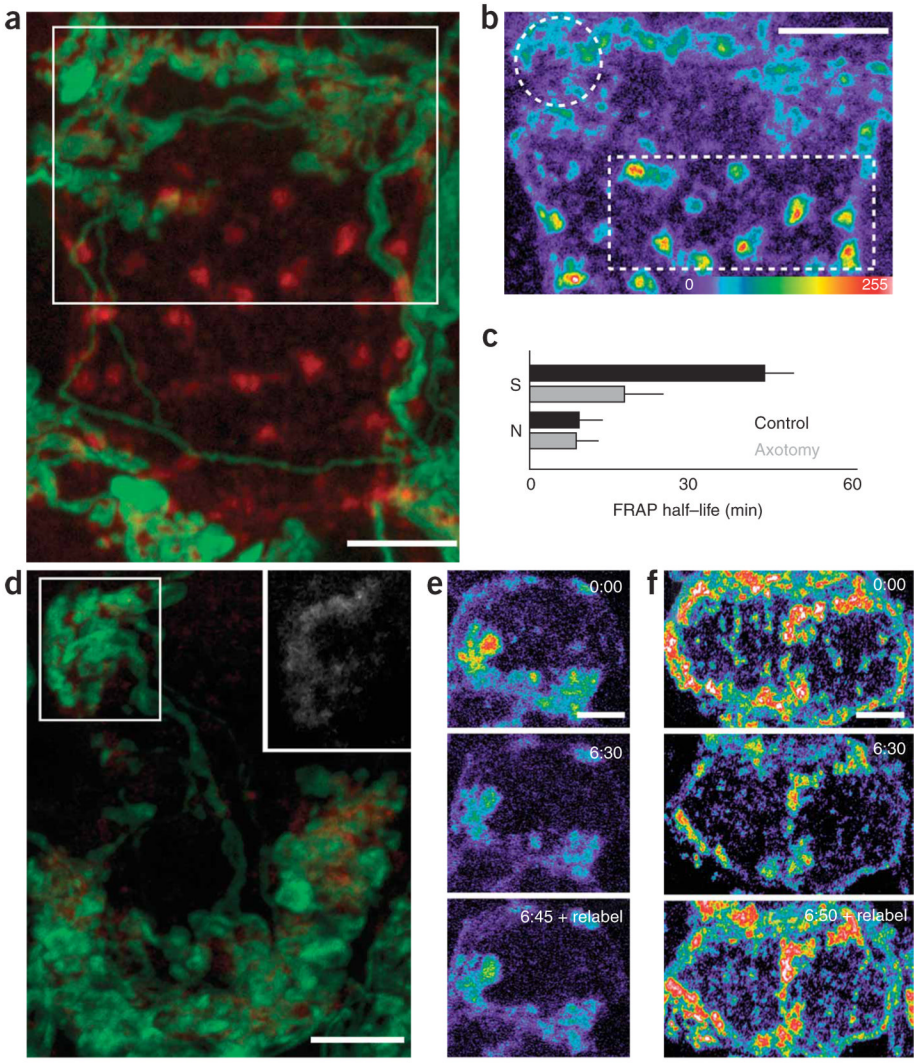

Figure 6. Altered distribution and dynamism of surface AChRs associated with AChR loss after axotomy

(**a**) Confocal reconstruction of the surface AChRs (red) and nerve terminal (green) of a ganglion cell 24 h after axotomy. (**b**) AChRs (red in **a**), pseudocolored, from the boxed region in **a**. Synaptic AChRs (circle) appear dimmer than nonsynaptic AChR clusters (square). (**c**) Pooled data from multiple experiments depicting the half-time of FRAP recovery for synaptic AChRs (S) and nonsynaptic AChRs (N) for control cells (black bars) versus cells 24 h after axotomy (gray bars). Error bars, s.e.m. (**d**) Confocal stack of a postganglionic neuron 48 h after axotomy. Dim BTX labeling (red) can still be found apposed to presynaptic terminals (green). Inset, enhanced image of BTX labeling from the boxed region in the upper left position of **d** shows remaining AChRs. (**e**) Time-lapse imaging of BTX-labeled AChRs 36 h after axotomy shows disequilibrium between removal and insertion of AChRs. (**f**) Fluorescence decay and relabeling intensity in a control ganglion cell. In control (**f**) and axotomized cells (**e**), surface labeling grew dim over the course of hours (compare the first images at time 0 to the second images taken 6 h 30 min later). However, after axotomy, relabeling of newly inserted AChRs produced only a small increase in receptor fluorescence (see 6:45 + relabel), whereas fluorescence

intensity recovered to initial levels in control cells (see 6:50 + relabel). Scale bars, 5 μm in all images.

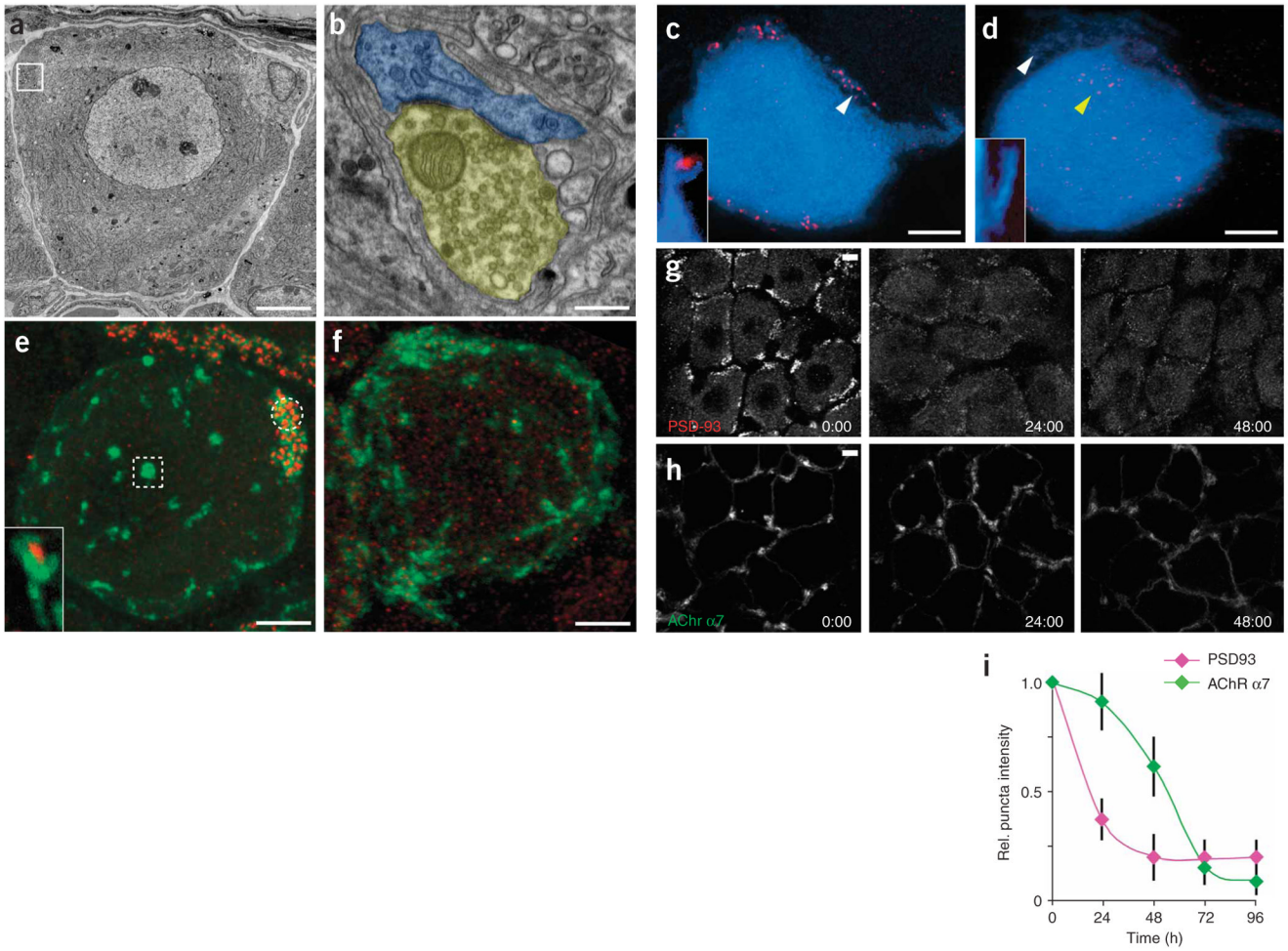

Figure 7. Loss of PSD-93 from postsynaptic spines precedes axotomy induced AChR loss

(**a**) Electron micrograph of a normal ganglion cell. Boxed region contains synaptic contacts. (**b**) High-magnification view of the boxed region in **a** (yellow, presynaptic terminal boutons; blue, postsynaptic spines). (**c**) In a control ganglion cell (blue), PSD-93 is localized to small spines that protrude from the cell surface (white arrow and inset). (**d**) By 36 h after axotomy, many spines no longer contained PSD-93 labeling (white arrow and inset) and cells now contained mislocalized PSD-93 puncta (yellow arrow). (**e**) In normal ganglion cells, PSD-93 (red) colocalized with synaptic AChR α7 (green labeling, circle) but was not found at nonsynaptic clusters of AChR α7 (box). Inset, both PSD-93 and AChR α7 were present on small spines that extend from the cell surface. (**f**) Thirty-six hours after axotomy, PSD-93 (red) was no longer associated with any AChR α7 clusters (green). (**g**) Loss of PSD-93 occurs rapidly after axotomy. Loss is apparent by 24 h and progresses until 48 h after axotomy. (**h**) Loss of AChR α7 occurred more slowly than loss of PSD-93. (**i**) Loss of AChR α7 surface labeling was preceded by loss of PSD-93. Error bars, s.e.m. Scale bars, 5 μm in **a**,**c–h** and 0.2 μm in **b**.

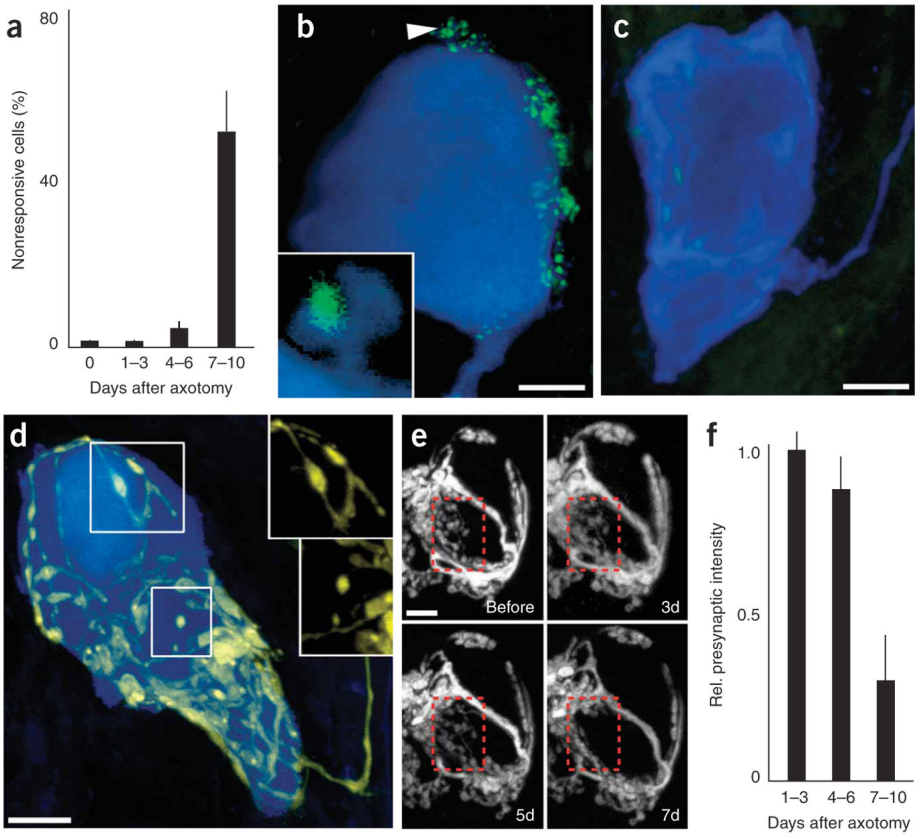

Figure 8. Delayed synapse elimination after postganglionic axotomy

(**a**) One week after postganglionic axotomy, about half of the postganglionic neurons no longer showed synaptic potentials in response to preganglionic stimulation. (**b**) Control postganglionic neurons (blue) possess small spines protruding from the cell surface (see arrow and inset). These spines colocalize with SV2, a marker for presynaptic terminals (green). (**c**) By 7 d after axotomy, postganglionic neurons showed few if any spines and presynaptic staining was no longer associated with the postsynaptic somata. (**d**) Preganglionic axon (yellow) that possessed retraction bulb–like structures (upper box) and disconnected axonal swellings (lower box) instead of the normal contiguous axonal wrapping. Insets, images of the preganglionic axons from the boxed regions in **d**. (**e**) Time-lapse imaging of preganglionic axons after postganglionic axotomy (enhanced to maximize contrast). By 7 d after axotomy, presynaptic terminals are lost (last image, red box). (**f**) Presynaptic fluorescence intensity was unchanged 1–3 d after axotomy, but was significantly reduced by 7–10 d after axotomy. Scale bars, 5 μm in all images. Error bars, s.e.m.